THE JOURNAL OF PHYSICAL CHEMISTRY A

pubs.acs.org/JPCA Article

Aqueous-Phase Decomposition of Isoprene Hydroxy Hydroperoxide and Hydroxyl Radical Formation by Fenton-like Reactions with Iron Ions

Ting Fang, Pascale S. J. Lakey, Jean C. Rivera-Rios, Frank N. Keutsch, and Manabu Shiraiwa*

Cite This: https://dx.doi.org/10.1021/acs.jpca.0c02094 Read Online

ACCESS | Metrics & More | Article Recommendations | Supporting Information

ABSTRACT: Isoprene hydroxy hydroperoxides (ISOPOOH) formed by the photooxidation of isoprene under low-NO conditions play an important role in the formation and evolution of secondary organic aerosols, yet multiphase processes of ISOPOOH are poorly understood. By applying electron paramagnetic resonance spectroscopy, we observe that ISOPOOH undergoes aqueous-phase decomposition upon interacting with Fe(II) ions to form OH and organic radicals at room temperature. To reproduce the measured dependence of OH formation on the Fe concentrations by kinetic modeling, we postulate that Fe(II) ions react with ISOPOOH via Fenton-like reactions to form OH radicals with a rate constant of 7.3×10^{-18} cm^3 s^{-1}. At low concentrations, oxalate forms monocomplexes with Fe(II) ions, which can promote OH formation by ISOPOOH. However, at high concentrations, oxalate scavenges OH radicals, thereby lowering aqueous OH concentrations. These findings provide new insight for the atmospheric fate of ISOPOOH and reactive oxygen species generation in the aqueous phase.

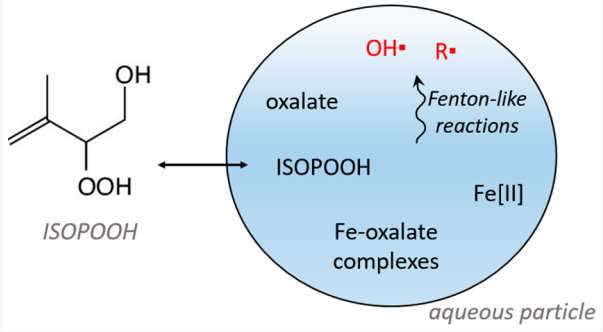

1. INTRODUCTION

Reactive oxygen species (ROS) trigger chemical reactions in the atmosphere, playing a central role in aerosol effects on climate, air quality, and public health.[1] OH radicals, the most reactive form of ROS, are of particular importance as they play a key role in chemical transformations of inorganic and organic compounds. Sources of OH in the aqueous phase include uptake from the gas phase,[2] H_2O_2 photolysis,[3,4] Fenton and photo-Fenton reactions,[5−8] and reactions with iron ions and peracids.[9] Recent studies have shown that the decomposition of secondary organic aerosols (SOA) in water can be a significant source of OH radicals under light[10] and dark[11−14] conditions. Organic hydroperoxides contained in SOA can decompose to release ROS upon interacting with transition-metal ions as well as quinones contained in humic-like substances.[13,15,16] Sources, sinks, and concentrations of OH radicals in atmospheric waters are very important because they control radical aqueous chemistry but are not quantified rigorously.[7,17−19]

One of the most abundant and important SOA precursors is isoprene (2-methyl-1,3-butadiene, C_5H_8), which is emitted from plants.[20] Isoprene undergoes atmospheric oxidation by OH radicals which under low-NO conditions leads to the formation of unsaturated hydroxy hydroperoxides (ISOPOOH). Further oxidation of ISOPOOH by OH produces isoprene epoxydiols (IEPOX),[21] and the subsequent multiphase chemistry of IEPOX leads to substantial SOA formation.[22−25] Previous studies have shown that isoprene-derived SOA can cause the formation of OH radicals upon interacting with water and Fe(II).[12,13] The fate and multiphase processes of ISOPOOH are yet to be elucidated.

Fe ions are redox-active and reactive toward hydrogen peroxide and organic hydroperoxides via Fenton(-like) chemistry to induce ROS formation,[5,9] affecting ROS concentrations in aqueous droplets.[14,26−29] A recent study suggests that the complex formation between Fe ions and SOA components may suppress OH formation by photo-Fenton chemistry.[30] Other recent studies suggest that humic-like substances can enhance OH formation due to the chemistry of the organic acid−Fe^{2+} complex.[31,32] The effect of metal−organic complexes on ROS formation is complex and hardly understood. In this study, we investigate the aqueous-phase chemistry of ISOPOOH with Fe ions and organic ligands to quantify the production of OH radicals.

Received: March 9, 2020
Revised: May 22, 2020
Published: June 1, 2020

2. MATERIALS AND METHODS

2.1. Experiments. Two major isomers of ISOPOOH, 4,3-ISOPOOH and 1,2-ISOPOOH, were synthesized in high purity (>99%).[33,34] A total of 60 μL of sample solution was mixed from the following chemicals in the order of 20 μL of ISOPOOH, 20 μL of BMPO, and 20 μL of Fe(II) or Fe(III) solution at room temperature (20−25 °C). BMPO (5-*tert*-butoxycarbonyl-5-methyl-1-pyrroline-*N*-oxide) is a spin-trapping agent that captures short-lived radicals including superoxides, hydroxyls, and carbon- and oxygen-centered organic radicals to form stable radical adducts.[35] For metal−organic complexation experiments, oxalic acid is chosen as a model organic ligand because it is an abundant organic constituent in atmospheric particles and a strong organic ligand that preferentially complexes with Fe(II) and Fe(III).[36] ISOPOOH (10 μL), oxalic acid (OA, 10 μL), BMPO (20 μL), and Fe(II) (20 μL) were mixed. The pH was not adjusted, and pH measurements showed that the final solution had a pH of between 2.5 and 4. A continuous-wave electron paramagnetic resonance (CW-EPR) spectrometer (Bruker, Germany) was used to detect the radical adducts at room temperature. Control experiments showed that ISOPOOH alone, OA alone, and Fe with OA in water do not generate any detectable radicals, so Fe(II) or Fe(III) was added last to initiate the radical-generating reaction (i.e., t = 0). The formation of the radical adducts and their temporal evolution was monitored. Each EPR spectrum was simulated by the Spin Fit module in the Xenon software to identify the radical adducts. The Spin Count module was further applied to quantify the concentrations of different radical adducts. Measurement uncertainties were assessed by repeating a subset of samples (N = 90) and are estimated to be 10% (Figure S1).

2.2. Kinetic Modeling. The concentrations of BMPO-OH and BMPO-R radical adducts were simulated using a kinetic box model with the mechanism in Table S1. The reactions in the model include reactions of ISOPOOH with Fe species (R18−R20) and OH radicals (R23 and R24), the formation of different radical adducts (R28−R32), the destruction of these adducts by self-decomposition (R33−R36), reactions with Fe(II) (R43) and radicals (R37−R42), radical−radical reactions (R16 and R44−R47), and Fe-oxalate complexation chemistry (R48−R69). For the majority of reactions, rate constants were based on literature values. Unknown or uncertain rate coefficients were determined using the Monte Carlo genetic algorithm (MCGA) method[37] and sensitivity studies. The MCGA method provides a high-performance optimization to constrain model input parameters using experimental data. It has been successfully used in the kinetic modeling of aerosol multiphase chemistry.[37] We applied the Visual MINTEQ 3.1 model[38] to estimate the equilibrium speciation of different Fe-oxalate complexes over the range of Fe and oxalate concentrations which were used during the experiments. For Fe(II), the speciation was determined at pH 3, while for Fe(III), the average speciation from pH 2.5 and 3.5 was determined by representing the variability during experiments. Equilibrium constants were calculated using the MINTEQ 3.1 speciation output and were then used to constrain one direction of the equilibrium reaction (R50, 51, 65, 67, and 69), so that the kinetic model is constrained by MINTEQ 3.1 at equilibrium.

3. RESULTS AND DISCUSSION

3.1. ROS Generation by ISOPOOH and Fe. Figure 1 shows an example of the time evolution of EPR spectra from

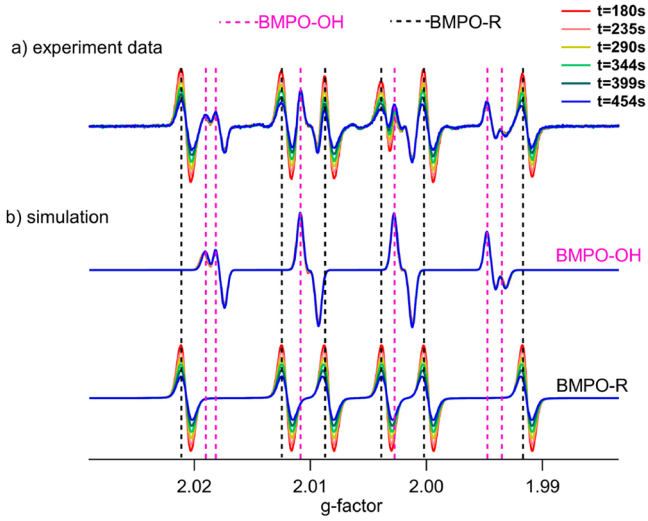

Figure 1. Examples of time-dependent (a) EPR spectra and (b) simulated spectra of BMPO-OH and BMPO-R adducts obtained from aqueous reactions of ISOPOOH with Fe(II). EPR spectra were recorded at various reaction times t from the initiation of the reaction by the addition of Fe(II). The vertical dashed lines indicate the characteristic peaks of BMPO-OH (pink) and BMPO-R (black) adducts.

the experiments and simulation based on aqueous reactions of ISOPOOH with Fe(II). The characteristic four- and six-line signals generated by the hyperfine splitting of BMPO-OH and BMPO-R adducts, respectively, indicate that ISOPOOH reacts with Fe(II) ions to form mainly OH and carbon-centered radicals in water. The fraction of BMPO-OH adducts shows a large variation (20−80%, median = 53%), depending on the initial concentrations of Fe(II) (Figure S2). In the absence of iron ions, ISOPOOH does not generate detectable amounts of any radicals in water. Note that previous studies have shown that isoprene SOA generate OH radicals dominantly and that the OH formation yield is enhanced in the presence of Fe(II).[13,14] It indicates that other organic hydroperoxides contained in isoprene SOA are more reactive than ISOPOOH and should be decomposed in water to form OH radicals.

Fe(III) is known to induce positive OH adduct artifacts in EPR measurements with DMPO, a nitric oxide spin trap similar to that of BMPO, through nucleophile substitution.[39] Similarly, Fe(III) can withdraw an electron from the double bond of BMPO, and water can attack the positively polarized double bond of BMPO, leading to a non-spin-trap production of BMPO-OH. Therefore, a set of EPR measurement on Fe(III) and BMPO only (i.e., no ISOPOOH) were used for baseline subtractions. After subtraction, BMPO-OH levels from the reactions between ISOPOOH and Fe(III) are low (Figure S3), indicating that radical formation by ISOPOOH + Fe(III) is not substantial.

Figure 2 shows experimental data and kinetic model simulations of the Fe(II)-concentration dependence of the BMPO-OH concentrations (Figure 2a) and the OH-forming efficiencies (i.e., molar concentration ratio of BMPO-OH and ISOPOOH in %) (Figure 2b) at different initial ISOPOOH concentrations at reaction time t = 290 s. Both 4,3-ISOPOOH

https://dx.doi.org/10.1021/acs.jpca.0c02094
J. Phys. Chem. A XXXX, XXX, XXX−XXX

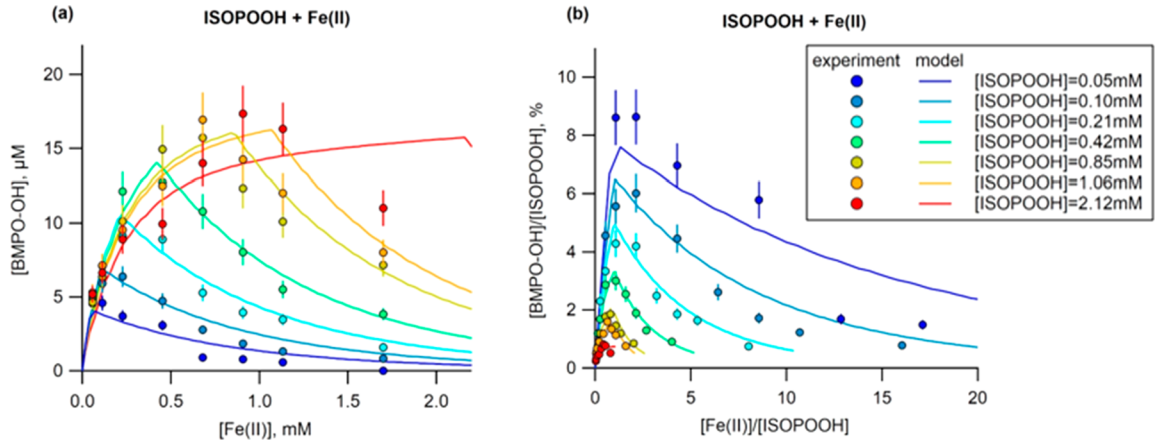

Figure 2. (a) Concentrations of OH radicals as trapped by BMPO in the aqueous reactions of 4,3-ISOPOOH with Fe(II) as a function of Fe concentrations. (b) OH formation efficiency (i.e., [BMPO−OH]/[ISOPOOH] in %) against [Fe(II)]/[ISOPOOH] at a reaction time of 290 s. The markers with error bars (10% uncertainty) are experimental data, and the solid lines represent kinetic model simulations.

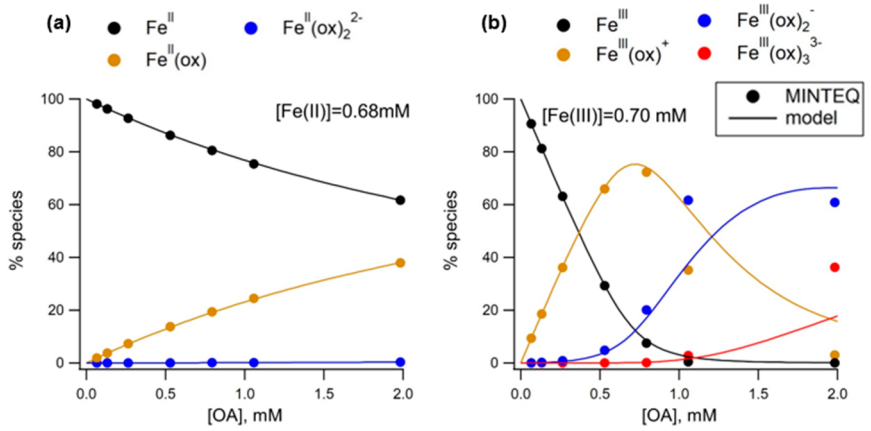

Figure 3. Speciation of (a) Fe(II) and (b) Fe(III) in Fe ions and oxalate solutions based on the MINTEQ 3.1 model (markers) and the kinetic model (lines). Fe(II) and Fe(III) are uncomplexed Fe ions. $Fe(ox)^{+}$, $Fe(ox)_2^{-}$, and $Fe(ox)_3^{3-}$ are Fe-forming complexes with one, two, and three oxalates, respectively. The solid lines indicate kinetic model outputs in the absence of ISOPOOH and oxygen.

and 1,2-ISOPOOH isomers show very similar trends in BMPO-OH and BMPO-R over the same ranges of Fe(II) and ISOPOOH concentrations (Figure S4), suggesting that radical formation from aqueous reactions of ISOPOOH and the Fe(II) ion does not depend on isomer types and a functional group plays a central role in radical formation. Hydroperoxide groups (ROOH) are known to react with Fe(II) via Fenton-like reactions, leading to the heterolytic cleavage of the O−O bond in two ways: one forms OH radicals (R18) and the other forms alkoxyl radicals (R19) as follows[13,40]

$$\mathrm{Fe(II)} + \mathrm{ISOPOOH} \rightarrow \mathrm{Fe(III)} + \mathrm{RO{-}{+}OH\cdot}$$
$$k_{18} = 7.3 \times 10^{-18}\,\mathrm{cm^3\,s^{-1}}\ (4.4 \times 10^{3}\,\mathrm{M^{-1}\,s^{-1}}) \qquad \text{(R18)}$$

$$\mathrm{Fe(II)} + \mathrm{ISOPOOH} \rightarrow \mathrm{Fe(III)} + \mathrm{RO\cdot} + \mathrm{OH{-}}$$
$$k_{19} = 6.6 \times 10^{-17}\,\mathrm{cm^3\,s^{-1}}\ (4.0 \times 10^{4}\,\mathrm{M^{-1}\,s^{-1}}) \qquad \text{(R19)}$$

where k is the rate coefficient determined from the MCGA optimization method. By implementing these two reactions in addition to other reactions as assembled in Table S1, the model reproduces experimental data within error bars over a wide range of ISOPOOH and Fe(II) concentrations as shown with the solid lines in Figure 2a. The comparisons at other reaction times also show good agreement (data not shown). Note that k_{18} is in the range (10^{-21}–6×10^{-17} $\mathrm{cm^3\,s^{-1}}$) and k_{19} is larger ($\sim 10^{-20}$ $\mathrm{cm^3\ s^{-1}}$) compared to previously reported rate coefficients for ROOH contained in different types of SOA.[13,14] The observed OH concentrations show a strong dependence on the concentration of Fe(II). BMPO-OH increases initially with an increase of Fe(II), which is due to faster turnover rates of R18 at higher Fe(II). BMPO-OH then decreases at higher Fe(II) concentrations, which can be explained by the decay of BMPO-OH by Fe(II) (R43 in Table S1).[14] Note that alkoxy (RO) radicals are formed in R19 but not detected, which may be due to the fast decomposition of RO radicals to form R radicals (R21). The trend in BMPO-R concentrations on different initial Fe ions or ISOPOOH concentrations is not clear (Figure. S5), probably due to R representing different organic radical species which may be generated via secondary reactions of OH with ISOPOOH. This makes the comparisons between the model and experimental results for BMPO-R challenging, although the model reproduces the experimental BMPO-R data to the same order of magnitude.

Fe(III) is known to oxidize the ROOH groups to form peroxy radicals (RO_2) and Fe(II) by a widely reported reaction: Fe(III) + ROOH → Fe(II) + RO_2 + H^+ (R20).[41,42] Further reactions of ROOH with Fe(II) (R18) generate OH

https://dx.doi.org/10.1021/acs.jpca.0c02094
J. Phys. Chem. A XXXX, XXX, XXX−XXX

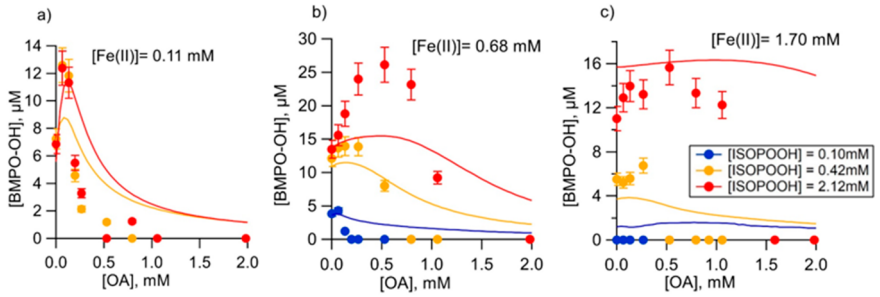

Figure 4. Effect of oxalic acid on the BMPO-OH adducts formed from BMPO trapping OH radicals generated in the aqueous reactions of 4,3-ISOPOOH with different Fe(II) concentrations ((a) 0.11, (b) 0.68, and (c) 1.70 mM) at a reaction time of 290 s. The markers with error bars (10% uncertainty) are experimental data, and the solid lines represent kinetic model simulations.

radicals. However, R20 is very slow ($k_{20} = 3.6 \times 10^{-23}$ cm^3 s^{-1}) and thus would not contribute substantially to OH generation. The much slower rate constant of R20 compared to those of R18 and R19 is consistent with the catalytic cycle of the Fenton reactions: Fe(III) + H_2O_2 → Fe(II) + HO_2 + H^+ (k_{11} = 3.3 × 10^{-24} cm^3 s^{-1})[43] is much slower than Fe(II) + H_2O_2 → Fe(III) + OH^- + OH (k_9 = 1.1 × 10^{-18} cm^3 s^{-1}).[44] Thus, a slow reaction of Fe(III) with ISOPOOH to generate Fe(II), which further reacts with ISOPOOH to form OH radicals, is consistent with the low OH formation from the Fe(III) reaction with ISOPOOH observed in our experiments.

3.2. Effect of Metal−Organic Complexation. We further investigated the effect of metal−organic complexation on OH production by ISOPOOH and Fe(II) with the addition of oxalic acid (OA). Figure 3 shows the Fe speciation from the kinetic model and the MINTEQ model at (a) [Fe(II)] = 0.68 mM and (b) [Fe(III)] = 0.70 mM. Fe(II) mainly forms a monocomplex ($Fe^{II}(ox)$) with oxalate (ox, $C_2O_4^{2-}$).[45] An increase in [OA] leads to a steady increase in [$Fe^{II}(ox)$] and a decrease in uncomplexed [Fe(II)] (Figure 3). Fe(III) can form mono-oxalate ($Fe^{III}(ox)^+$), dioxalate ($Fe^{III}(ox)_2^-$), or trioxalate ($Fe^{III}(ox)_3^{3-}$) complexes[46] depending on the concentrations of oxalate and Fe ions (Figure S6). At [OA] < [Fe(III)], an increase in [OA] leads to a decrease in uncomplexed [Fe(III)] and an increase in [$Fe^{III}(ox)^+$]; at [OA] > [Fe(III)], [$Fe^{III}(ox)^+$] decreases and $Fe^{III}(ox)_2^-$ and $Fe^{III}(ox)_3^{3-}$ start to form in the absence of uncomplexed Fe(III) (Figure 3).

Figure 4 shows [BMPO−OH] with three different initial ISOPOOH and Fe(II) concentrations and various OA concentrations. The addition of OA leads to a nonlinear response of BMPO−OH over different OA concentrations. At low [Fe(II)] (Figure 4a), [BMPO−OH] shows an initial increase followed by a sharp decrease to zero with increasing [OA]. The initial increase is likely due to the formation of Fe(II)-OA complexes. $Fe^{II}(ox)$ is known to act as a catalyst and accelerate the reaction of Fe(II) with H_2O_2.[47,48] Similarly, $Fe^{II}(ox)$ may increase the OH production of Fe(II) with ISOPOOH. The sharp decrease is likely due to oxalate competing with BMPO in the reaction with OH radicals (R63).[49] At medium and high [Fe(II)] with low [ISOPOOH] (Figure 4b,c), since most ISOPOOH is consumed by reacting with Fe(II), there is limited ISOPOOH available to react with the $Fe^{II}(ox)$ complex to form OH radicals. This leads to a smaller increase in [BMPO-OH] at initial [OA]. However, as [OA] increases, [BMPO-OH] follows the same decrease due to the radical-scavenging activity of oxalate. This suggests that OH formation is limited by ISOPOOH availability. In contrast, when Fe(II) and ISOPOOH are relatively abundant, substantial Fe(III) is formed via Fenton-like reactions R18 and R19. Fe(III) is more efficient in forming complexes with oxalate than Fe(II) (Figure S6 and S7),[46] thereby inhibiting oxalate from scavenging OH radicals. Thus, [BMPO-OH] can stay constant over a larger range of [OA].

By implementing the complex formation and associated chemical reactions (Table S1), the model reproduces the observed OH formation reasonably well. However, it still could not fully explain the initial increases in [BMPO-OH] at high [ISOPOOH] and medium [Fe(II)] (Figure 4b). This indicates that additional OH sources related to ISOPOOH may still be missing, which needs to be further investigated to fully elucidate the chemistry of Fe complexes. Nevertheless, these experimental and modeling results demonstrate the complex behavior and effects of multicomponent mixtures on ROS formation: organic compounds that can act as polydentate ligands can promote the Fenton-like reactions.

The findings of this study have significant implications on the atmospheric fate of ISOPOOH. ISOPOOH has been mainly regarded as an important precursor of IEPOX that triggers multiphase processes, but this study suggests that ISOPOOH itself can trigger aqueous chemistry by forming OH and RO radicals. RO radicals may further decompose to form stable products such as methyl vinyl ketone, methacrolein, and formaldehyde.[33] With typical ambient gas-phase ISOPOOH concentrations of 10−200 pptv[50] and a Henry's law constant of 1.17 × 10^4 M atm^{-1} for 4,3-ISOPOOH, aqueous concentrations of ISOPOOH are estimated to be 0.1−2.5 nM. Considering typical aqueous Fe concentrations of 10^{-3}−40 μM,[27] the OH production rates from ISOPOOH reacting with Fe are estimated to be in the range of 10^{-4}−1 pM s^{-1}. Even though ISOPOOH decomposition should be a minor source of OH radicals compared to other sources,[9] the formed OH radicals should participate in reactions with surrounding organic molecules to induce chemical transformation. These aqueous-phase processes can be further complicated by the complexation state of Fe ions. In the presence of oxalic acid with typical concentrations of 0.18−12 μM,[51,52] kinetic modeling predicts that the OH production rates increase up to 2 pM s^{-1} (double the OH production rate estimated without oxalic acid) (Figure S8). Aqueous OH concentrations are controlled by a complexation-mediated increase in production rates as well as the scavenging activity of oxalate. It should be noted that although oxalate is an abundant aerosol constituent and a strong organic ligand,[36] other metal-complexing organic acids may also play a role in OH production from ISOPOOH and Fe Fenton-like reactions under atmospheric conditions.

https://dx.doi.org/10.1021/acs.jpca.0c02094
J. Phys. Chem. A XXXX, XXX, XXX−XXX

4. CONCLUSIONS

ISOPOOH formed by isoprene photooxidation plays an important role in the formation and chemical transformation of secondary organic aerosols, but the fate of ISOPOOH in aqueous droplets has been poorly understood. In this study, we investigated the decomposition of ISOPOOH and formation of ROS in the aqueous phase with and without iron ions at room temperature using electron paramagnetic resonance spectroscopy combined with a spin-trapping technique. We found that ISOPOOH is stable in the aqueous phase and no ROS formation is observed in the absence of iron ions. In aqueous mixtures of ISOPOOH and Fe(II) ions, it is shown that OH and organic radicals are formed, while ROS formation is insignificant for mixtures of ISOPOOH and Fe(III) ions. The ROS formation dependence on the concentrations of ISOPOOH and Fe(II) can be reproduced by kinetic modeling by considering Fenton-like reactions between ISOPOOH and Fe(II) ions as well as ROS and spin-trapping reactions. We further investigated the effect of metal−organic complexation on OH production by ISOPOOH and Fe(II) with the addition of oxalic acid. At low concentrations, oxalate forms monocomplexes with Fe(II) ions, leading to the promotion of OH formation; however, at high oxalate concentrations, the scavenging of OH radicals by oxalate results in a lowering of the aqueous OH concentrations. This work highlights ROS generation and the role of metal−organic complexation in the Fenton-like reactions of ISOPOOH and Fe(II) ions, providing new insight for the atmospheric fate of ISOPOOH in the aqueous phase. Further work is necessary to elucidate the role and impact of generated ROS by ISOPOOH on the aqueous-phase processing of organic aerosols in the atmosphere.

■ ASSOCIATED CONTENT

Supporting Information

The Supporting Information is available free of charge at https://pubs.acs.org/doi/10.1021/acs.jpca.0c02094.

Chemical information and electron paramagnetic resonance measurements, Table S1, and Figures S1−S8 (PDF)

■ AUTHOR INFORMATION

Corresponding Author

Manabu Shiraiwa − *Department of Chemistry, University of California, Irvine, California 92697, United States;* orcid.org/0000-0003-2532-5373; Phone: +1 949-824-2738; Email: m.shiraiwa@uci.edu

Authors

Ting Fang − *Department of Chemistry, University of California, Irvine, California 92697, United States;* orcid.org/0000-0002-4845-2749

Pascale S. J. Lakey − *Department of Chemistry, University of California, Irvine, California 92697, United States*

Jean C. Rivera-Rios − *Department of Chemistry and Chemical Biology, Harvard University, Cambridge, Massachusetts 02138, United States*

Frank N. Keutsch − *Department of Chemistry and Chemical Biology and Harvard John A. Paulson School of Engineering and Applied Sciences, Department of Earth and Planetary Sciences, Harvard University, Cambridge, Massachusetts 02138, United States*

Complete contact information is available at: https://pubs.acs.org/10.1021/acs.jpca.0c02094

Notes

The authors declare no competing financial interest.

■ ACKNOWLEDGMENTS

This work was funded by the National Science Foundation (CHE-1808125). The authors thank Thomas Berkemeier (Max Planck Institute for Chemistry) for sharing the code of the Monte Carlo genetic algorithm (MCGA) method. We thank Hind Al-Abadleh (Wilfrid Laurier University) for helpful discussions.

■ REFERENCES

(1) Pöschl, U.; Shiraiwa, M. Multiphase Chemistry at the Atmosphere-Biosphere Interface Influencing Climate and Public Health in the Anthropocene. *Chem. Rev.* **2015**, *115* (10), 4440−4475.

(2) Herrmann, H.; Hoffmann, D.; Schaefer, T.; Bräuer, P.; Tilgner, A. Tropospheric Aqueous-Phase Free-Radical Chemistry: Radical Sources, Spectra, Reaction Kinetics and Prediction Tools. *ChemPhysChem* **2010**, *11* (18), 3796−3822.

(3) Jacob, D. J. Chemistry of OH in Remote Clouds and Its Role in the Production of Formic Acid and Peroxymonosulfate. *J. Geophys. Res.* **1986**, *91* (D9), 9807−9826.

(4) Bianco, A.; Passananti, M.; Perroux, H.; Voyard, G.; Mouchel-Vallon, C.; Chaumerliac, N.; Mailhot, G.; Deguillaume, L.; Brigante, M. A Better Understanding of Hydroxyl Radical Photochemical Sources in Cloud Waters Collected at the Puy De Dôme Station - Experimental versus Modelled Formation Rates. *Atmos. Chem. Phys.* **2015**, *15* (16), 9191−9202.

(5) Fenton, H. J. H. LXXIII.—Oxidation of Tartaric Acid in Presence of Iron. *J. Chem. Soc., Trans.* **1894**, *65*, 899−910.

(6) Herrmann, H.; Tilgner, A.; Barzaghi, P.; Majdik, Z.; Gligorovski, S.; Poulain, L.; Monod, A. Towards a More Detailed Description of Tropospheric Aqueous Phase Organic Chemistry: CAPRAM 3.0. *Atmos. Environ.* **2005**, *39* (23−24), 4351−4363.

(7) Ervens, B. Modeling the Processing of Aerosol and Trace Gases in Clouds and Fogs. *Chem. Rev.* **2015**, *115* (10), 4157−4198.

(8) Arakaki, T.; Anastasio, C.; Kuroki, Y.; Nakajima, H.; Okada, K.; Kotani, Y.; Handa, D.; Azechi, S.; Kimura, T.; Tsuhako, A.; Miyagi, Y. A General Scavenging Rate Constant for Reaction of Hydroxyl Radical with Organic Carbon in Atmospheric Waters. *Environ. Sci. Technol.* **2013**, *47* (15), 8196−8203.

(9) Paulson, S. E.; Gallimore, P. J.; Kuang, X. M.; Chen, J. R.; Kalberer, M.; Gonzalez, D. H. A Light-Driven Burst of Hydroxyl Radicals Dominates Oxidation Chemistry in Newly Activated Cloud Droplets. *Sci. Adv.* **2019**, *5* (5), No. eaav7689.

(10) Badali, K. M.; Zhou, S.; Aljawhary, D.; Antiñolo, M.; Chen, W. J.; Lok, A.; Mungall, E.; Wong, J. P. S.; Zhao, R.; Abbatt, J. P. D. Formation of Hydroxyl Radicals from Photolysis of Secondary Organic Aerosol Material. *Atmos. Chem. Phys.* **2015**, *15* (14), 7831−7840.

(11) Lim, Y. B.; Turpin, B. J. Laboratory Evidence of Organic Peroxide and Peroxyhemiacetal Formation in the Aqueous Phase and Implications for Aqueous OH. *Atmos. Chem. Phys.* **2015**, *15* (22), 12867−12877.

(12) Tong, H.; Lakey, P. S. J.; Arangio, A. M.; Socorro, J.; Shen, F.; Lucas, K.; Brune, W. H.; Pöschl, U.; Shiraiwa, M. Reactive Oxygen Species Formed by Secondary Organic Aerosols in Water and Surrogate Lung Fluid. *Environ. Sci. Technol.* **2018**, *52* (20), 11642−11651.

(13) Tong, H.; Arangio, A. M.; Lakey, P. S. J.; Berkemeier, T.; Liu, F.; Kampf, C. J.; Brune, W. H.; Pöschl, U.; Shiraiwa, M. Hydroxyl Radicals from Secondary Organic Aerosol Decomposition in Water. *Atmos. Chem. Phys.* **2016**, *16* (3), 1761−1771.

(14) Tong, H.; Lakey, P. S. J.; Arangio, A. M.; Socorro, J.; Kampf, C. J.; Berkemeier, T.; Brune, W. H.; Poschl, U.; Shiraiwa, M. Reactive

Oxygen Species Formed in Aqueous Mixtures of Secondary Organic Aerosols and Mineral Dust Influencing Cloud Chemistry and Public Health in the Anthropocene. *Faraday Discuss.* **2017**, *200*, 251−270.
(15) Arangio, A. M.; Tong, H.; Socorro, J.; Pöschl, U.; Shiraiwa, M. Quantification of Environmentally Persistent Free Radicals and Reactive Oxygen Species in Atmospheric Aerosol Particles. *Atmos. Chem. Phys.* **2016**, *16* (20), 13105−13119.
(16) Tong, H.; Zhang, Y.; Filippi, A.; Wang, T.; Li, C.; Liu, F.; Leppla, D.; Kourtchev, I.; Wang, K.; Keskinen, H.-M.; Levula, J. T.; Arangio, A. M.; Shen, F.; Ditas, F.; Martin, S. T.; Artaxo, P.; Godoi, R. H. M.; Yamamoto, C. I.; de Souza, R. A. F.; Huang, R.-J.; Berkemeier, T.; Wang, Y.; Su, H.; Cheng, Y.; Pope, F. D.; Fu, P.; Yao, M.; Pöhlker, C.; Petäjä, T.; Kulmala, M.; Andreae, M. O.; Shiraiwa, M.; Pöschl, U.; Hoffmann, T.; Kalberer, M. Radical Formation by Fine Particulate Matter Associated with Highly Oxygenated Molecules. *Environ. Sci. Technol.* **2019**, *53* (21), 12506−12518.
(17) Herrmann, H.; Schaefer, T.; Tilgner, A.; Styler, S. A.; Weller, C.; Teich, M.; Otto, T. Tropospheric Aqueous-Phase Chemistry: Kinetics, Mechanisms, and Its Coupling to a Changing Gas Phase. *Chem. Rev.* **2015**, *115* (10), 4259−4334.
(18) Carlton, A. G.; Wiedinmyer, C.; Kroll, J. H. A Review of Secondary Organic Aerosol (SOA) Formation from Isoprene. *Atmos. Chem. Phys.* **2009**, *9* (14), 4987−5005.
(19) Ervens, B.; Turpin, B. J.; Weber, R. J. Secondary Organic Aerosol Formation in Cloud Droplets and Aqueous Particles (aqSOA): a Review of Laboratory, Field and Model Studies. *Atmos. Chem. Phys.* **2011**, *11* (21), 11069−11102.
(20) Guenther, A. B.; Jiang, X.; Heald, C. L.; Sakulyanontvittaya, T.; Duhl, T.; Emmons, L. K.; Wang, X. The Model of Emissions of Gases and Aerosols from Nature Version 2.1 (MEGAN2.1): an Extended and Updated Framework for Modeling Biogenic Emissions. *Geosci. Model Dev.* **2012**, *5* (6), 1471−1492.
(21) Paulot, F.; Crounse, J. D.; Kjaergaard, H. G.; Kurten, A.; St Clair, J. M.; Seinfeld, J. H.; Wennberg, P. O. Unexpected Epoxide Formation in the Gas-Phase Photooxidation of Isoprene. *Science* **2009**, *325* (5941), 730−733.
(22) Nguyen, T. B.; Coggon, M. M.; Bates, K. H.; Zhang, X.; Schwantes, R. H.; Schilling, K. A.; Loza, C. L.; Flagan, R. C.; Wennberg, P. O.; Seinfeld, J. H. Organic Aerosol Formation from the Reactive Uptake of Isoprene Epoxydiols (IEPOX) onto Non-acidified Inorganic Seeds. *Atmos. Chem. Phys.* **2014**, *14* (7), 3497−3510.
(23) Lin, Y.-H.; Zhang, Z.; Docherty, K. S.; Zhang, H.; Budisulistiorini, S. H.; Rubitschun, C. L.; Shaw, S. L.; Knipping, E. M.; Edgerton, E. S.; Kleindienst, T. E.; Gold, A.; Surratt, J. D. Isoprene Epoxydiols as Precursors to Secondary Organic Aerosol Formation: Acid-Catalyzed Reactive Uptake Studies with Authentic Compounds. *Environ. Sci. Technol.* **2012**, *46* (1), 250−258.
(24) Worton, D. R.; Surratt, J. D.; LaFranchi, B. W.; Chan, A. W. H.; Zhao, Y.; Weber, R. J.; Park, J.-H.; Gilman, J. B.; de Gouw, J.; Park, C.; Schade, G.; Beaver, M.; Clair, J. M. S.; Crounse, J.; Wennberg, P.; Wolfe, G. M.; Harrold, S.; Thornton, J. A.; Farmer, D. K.; Docherty, K. S.; Cubison, M. J.; Jimenez, J.-L.; Frossard, A. A.; Russell, L. M.; Kristensen, K.; Glasius, M.; Mao, J.; Ren, X.; Brune, W.; Browne, E. C.; Pusede, S. E.; Cohen, R. C.; Seinfeld, J. H.; Goldstein, A. H. Observational Insights into Aerosol Formation from Isoprene. *Environ. Sci. Technol.* **2013**, *47* (20), 11403−11413.
(25) Surratt, J. D.; Chan, A. W. H.; Eddingsaas, N. C.; Chan, M. N.; Loza, C. L.; Kwan, A. J.; Hersey, S. P.; Flagan, R. C.; Wennberg, P. O.; Seinfeld, J. H. Reactive Intermediates Revealed in Secondary Organic Aerosol Formation from Isoprene. *Proc. Natl. Acad. Sci. U. S. A.* **2010**, *107* (15), 6640−6645.
(26) Arakaki, T.; Faust, B. C. Sources, Sinks, and Mechanisms of Hydroxyl Radical (•OH) Photoproduction and Consumption in Authentic Acidic Continental Cloud Waters from Whiteface Mountain, New York: The Role of the Fe(r) (r = II, III) Photochemical Cycle. *J. Geophys. Res.: Atmos.* **1998**, *103* (D3), 3487−3504.
(27) Deguillaume, L.; Leriche, M.; Desboeufs, K.; Mailhot, G.; George, C.; Chaumerliac, N. Transition Metals in Atmospheric Liquid Phases: Sources, Reactivity, and Sensitive Parameters. *Chem. Rev.* **2005**, *105* (9), 3388−3431.
(28) Lakey, P. S.; Berkemeier, T.; Tong, H.; Arangio, A. M.; Lucas, K.; Poschl, U.; Shiraiwa, M. Chemical Exposure-response Relationship between Air Pollutants and Reactive Oxygen Species in the Human Respiratory Tract. *Sci. Rep.* **2016**, *6*, 32916.
(29) Charrier, J. G.; McFall, A. S.; Richards-Henderson, N. K.; Anastasio, C. Hydrogen Peroxide Formation in a Surrogate Lung Fluid by Transition Metals and Quinones Present in Particulate Matter. *Environ. Sci. Technol.* **2014**, *48* (12), 7010−7017.
(30) Hems, R. F.; Hsieh, J. S.; Slodki, M. A.; Zhou, S.; Abbatt, J. P. D. Suppression of OH Generation from the Photo-Fenton Reaction in the Presence of α-Pinene Secondary Organic Aerosol Material. *Environ. Sci. Technol. Lett.* **2017**, *4* (10), 439−443.
(31) Wei, J.; Yu, H.; Wang, Y.; Verma, V. Complexation of Iron and Copper in Ambient Particulate Matter and Its Effect on the Oxidative Potential Measured in a Surrogate Lung Fluid. *Environ. Sci. Technol.* **2019**, *53* (3), 1661−1671.
(32) Gonzalez, D. H.; Cala, C. K.; Peng, Q.; Paulson, S. E. HULIS Enhancement of Hydroxyl Radical Formation from Fe(II): Kinetics of Fulvic Acid-Fe(II) Complexes in the Presence of Lung Antioxidants. *Environ. Sci. Technol.* **2017**, *51* (13), 7676−7685.
(33) Rivera-Rios, J. C.; Nguyen, T. B.; Crounse, J. D.; Jud, W.; St Clair, J. M.; Mikoviny, T.; Gilman, J. B.; Lerner, B. M.; Kaiser, J. B.; de Gouw, J.; Wisthaler, A.; Hansel, A.; Wennberg, P. O.; Seinfeld, J. H.; Keutsch, F. N. Conversion of Hydroperoxides to Carbonyls in Field and Laboratory Instrumentation: Observational Bias in Diagnosing Pristine versus Anthropogenically Controlled Atmospheric Chemistry. *Geophys. Res. Lett.* **2014**, *41* (23), 8645−8651.
(34) Maurya, R. A.; Park, C. P.; Kim, D.-P. Triple-channel Microreactor for Biphasic Gas-Liquid Reactions: Photosensitized Oxygenations. *Beilstein J. Org. Chem.* **2011**, *7* (1), 1158−1163.
(35) Zhao, H.; Joseph, J.; Zhang, H.; Karoui, H.; Kalyanaraman, B. Synthesis and Biochemical Applications of a Solid Cyclic Nitrone Spin Trap: a Relatively Superior Trap for Detecting Superoxide Anions and Glutathiyl Radicals. *Free Radical Biol. Med.* **2001**, *31* (5), 599−606.
(36) Al-Abadleh, H. A. Review of the Bulk and Surface Chemistry of Iron in Atmospherically Relevant Systems Containing Humic-like Substances. *RSC Adv.* **2015**, *5* (57), 45785−45811.
(37) Berkemeier, T.; Ammann, M.; Krieger, U. K.; Peter, T.; Spichtinger, P.; Pöschl, U.; Shiraiwa, M.; Huisman, A. J. Technical Note: Monte Carlo Genetic Algorithm (MCGA) for Model Analysis of Multiphase Chemical Kinetics to Determine Transport and Reaction Rate Coefficients using Multiple Experimental Data Sets. *Atmos. Chem. Phys.* **2017**, *17* (12), 8021−8029.
(38) Gustafsson, J. P., Visual MINTEQ 3.1. *Department of Land and Water Resources Engineering*; Royal Institute of Technology, Stockholm, 2012.
(39) Makino, K.; Hagiwara, T.; Hagi, A.; Nishi, M.; Murakami, A. Cautionary Note for DMPO Spin Trapping in the Presence of Iron Ion. *Biochem. Biophys. Res. Commun.* **1990**, *172* (3), 1073−1080.
(40) Goldstein, S.; Meyerstein, D. Comments on the Mechanism of the "Fenton-like" Reaction. *Acc. Chem. Res.* **1999**, *32* (7), 547−550.
(41) Halliwell, B.; Gutteridge, J. M. C. *Free Radicals in Biology and Medicine*. Oxford University Press: 2015.
(42) Repetto, M.; Semprine, J.; Boveris, A. *Lipid Peroxidation: Chemical Mechanism, Biological Implications and Analytical Determination*. IntechOpen: 2012; Vol. *1*.
(43) Lewis, S.; Lynch, A.; Bachas, L.; Hampson, S.; Ormsbee, L.; Bhattacharyya, D. Chelate-Modified Fenton Reaction for the Degradation of Trichloroethylene in Aqueous and Two-Phase Systems. *Environ. Eng. Sci.* **2009**, *26* (4), 849−859.
(44) Bataineh, H.; Pestovsky, O.; Bakac, A. pH-induced Mechanistic Changeover from Hydroxyl Radicals to Iron(IV) in the Fenton Reaction. *Chem. Sci.* **2012**, *3* (5), 1594−1599.
(45) Park, J. S. B.; Wood, P. M.; Davies, M. J.; Gilbert, B. C.; Whitwood, A. C. A Kinetic and ESR Investigation of Iron(II) Oxalate Oxidation by Hydrogen Peroxide and Dioxygen as a Source of Hydroxyl Radicals. *Free Radical Res.* **1997**, *27* (5), 447−458.

https://dx.doi.org/10.1021/acs.jpca.0c02094
J. Phys. Chem. A XXXX, XXX, XXX−XXX

(46) Tao, Y.; Murphy, J. G. The Mechanisms Responsible for the Interactions among Oxalate, pH, and Fe Dissolution in PM2.5. *ACS Earth Space Chem.* **2019**, *3* (10), 2259−2265.
(47) Pignatello, J. J.; Oliveros, E.; MacKay, A. Advanced Oxidation Processes for Organic Contaminant Destruction Based on the Fenton Reaction and Related Chemistry. *Crit. Rev. Environ. Sci. Technol.* **2006**, *36* (1), 1−84.
(48) Zuo, Y.; Hoigne, J. Formation of Hydrogen Peroxide and Depletion of Oxalic Acid in Atmospheric Water by Photolysis of Iron(III)-oxalato Complexes. *Environ. Sci. Technol.* **1992**, *26* (5), 1014−1022.
(49) Varela, E.; Tien, M. Effect of pH and Oxalate on Hydroquinone-Derived Hydroxyl Radical Formation during Brown Rot Wood Degradation. *Appl. Environ. Microbiol.* **2003**, *69* (10), 6025.
(50) Krechmer, J. E.; Coggon, M. M.; Massoli, P.; Nguyen, T. B.; Crounse, J. D.; Hu, W.; Day, D. A.; Tyndall, G. S.; Henze, D. K.; Rivera-Rios, J. C.; Nowak, J. B.; Kimmel, J. R.; Mauldin, R. L.; Stark, H.; Jayne, J. T.; Sipilä, M.; Junninen, H.; St. Clair, J. M.; Zhang, X.; Feiner, P. A.; Zhang, L.; Miller, D. O.; Brune, W. H.; Keutsch, F. N.; Wennberg, P. O.; Seinfeld, J. H.; Worsnop, D. R.; Jimenez, J. L.; Canagaratna, M. R. Formation of Low Volatility Organic Compounds and Secondary Organic Aerosol from Isoprene Hydroxyhydroperoxide Low-NO Oxidation. *Environ. Sci. Technol.* **2015**, *49* (17), 10330−10339.
(51) Crahan, K. K.; Hegg, D.; Covert, D. S.; Jonsson, H. An Exploration of Aqueous Oxalic Acid Production in the Coastal Marine Atmosphere. *Atmos. Environ.* **2004**, *38* (23), 3757−3764.
(52) Deutsch, F.; Hoffmann, P.; Ortner, H. M. Field Experimental Investigations on the Fe(II)- and Fe(III)-Content in Cloudwater Samples. *J. Atmos. Chem.* **2001**, *40* (1), 87−105.

https://dx.doi.org/10.1021/acs.jpca.0c02094
J. Phys. Chem. A XXXX, XXX, XXX−XXX